Journal of Sound and Vibration (2000) **233**(3), 369–389
doi:10.1006/jsvi.1999.2812, available online at http://www.idealibrary.com on IDEAL®

ENERGY FLOW MODELS FROM FINITE ELEMENT ANALYSIS

B. R. MACE AND P. J. SHORTER*

Department of Mechanical Engineering, University of Auckland, Private Bag 92019, *Auckland, New Zealand*

(*Received* 11 *June* 1998, *and in final form* 1 *February* 1999)

Computationally efficient methods are described by which the results of a finite element analysis of a system may be post-processed to form energy flow models, yielding time and, perhaps, frequency average subsystem energies as well as input and dissipated powers. The methods are particularly efficient for excitation which is spatially distributed or broadband (e.g., rain-on-the-roof) or if the frequency average response is required. First a method based on a global finite element analysis is presented. This involves a global modal decomposition and a reordering of the subsequent numerical calculations. The properties of the distribution of the excitation and the system's mass and stiffness lead to subsystem force distribution, mass distribution and stiffness distribution matrices. The response is given by a sum of terms involving the interaction of a pair of global modes, the contribution of each pair depending on the appropriate elements of the distribution matrices. Frequency averaging is performed by separating the resulting frequency-dependent terms and integrating. In most practical cases this integration can be done analytically. Next an alternative method involving component mode synthesis is described. In this, individual finite element analyses are performed for each subsystem using, here, the fixed interface method. These are then assembled to perform a global modal analysis, with the order of the model being much reduced. The consequent results are then post-processed in the same way. Finally, a system comprising three coupled plates is presented as a numerical example.

© 2000 Academic Press

1. INTRODUCTION

At lower frequencies, the dynamic behaviour of a structure is often expressed in terms of the magnitude and phase of the response at discrete frequencies and discrete locations. At higher frequencies, when high order modes contribute to the response, difficulties arise. The response of the system becomes sensitive to small details in its construction, its properties and its boundary conditions, which are not known to sufficient accuracy. Energy-based approaches such as statistical energy analysis (SEA) are therefore often adopted.

Energy flow methods give a "broad-brush" description of the dynamic behaviour of a structure. The system is divided into a (relatively small) number of coupled subsystems and the response to broadband excitation described in terms of the time and, normally, frequency average kinetic, potential and total energy in each subsystem, the energy flows between them and the input powers.

This paper concerns how energy flow models may be formed from finite element analysis (FEA). Various systematic and numerically efficient techniques are described by which the time and frequency average subsystem powers and energies may be determined. The

* Now at Vibro-Acoustic Sciences Inc., 12555 High Bluff Drive, Suite 310, San Diego, CA 92130, USA.

0022-460X/00/230369 + 21 $35.00/0 © 2000 Academic Press

reasons why this may be performed include the following. First, one might wish to construct an energy flow model of a specific system, under the assumption that the (broadband) frequency average response of the chosen system is indicative of that of any similar system. One might also use such a model to conduct numerical experiments in order to estimate parameters such as the SEA coupling loss factors between connected subsystems. Alternatively, one may intend to explore situations where the accuracy of methods such as SEA is suspect, for example if the coupling is strong, if there are only a few modes of one or more subsystems in the frequency band of interest or if there is only moderate uncertainty in the subsystem properties. Finally, deterministic analysis of a single system may be used as the basis for the study of the response statistics of a population of systems.

Applications of FEA to energy flow modelling are not new. Lyon [1] suggested the use of FEA in predicting SEA coupling loss factors during the early development of SEA. Various studies [2–6] have viewed the response of a finite element model in terms of an energy flow model. In all these studies a global FEA was performed on the system. The use of a lumped mass formulation is implicitly assumed and the kinetic energy found from a single summation involving the nodal mass and nodal velocity of responding nodes. Shankar and Keane [7, 8] develop an alternative "local" method, a receptance approach in which the response of each subsystem is described by Green functions. These are given by sums of subsystem modes which are found by analyzing each subsystem in turn with the coupling interfaces free. The uncoupled modes may be found analytically [7] or using FEA [8]. Such an approach substantially reduces the computational effort, requiring a number of smaller finite element analyses, while the size of the model used to calculate the forced response depends on the number of coupling degrees of freedom. While the approach allows for localized damping, it is limited to excitation at discrete frequencies and a number of discrete locations.

The finite element method has also been used to calculate structural intensity [10, 11]. Since intensity requires an accurate description of various spatial derivatives, a large number of modes are needed for convergence. Furthermore, since the intensity is sensitive to the relative phases of these modes, the predictions are potentially very sensitive to the accuracy of the data used to describe the system and to FEA discretization errors.

In this paper, computationally efficient methods of determining an energy flow model from a deterministic FEA are described. The methods require the subsystem mass and stiffness matrices to be found. This may be performed by any FEA package. Then a single, global modal analysis is performed, as described in the next section (a component mode approach is described later). The results of the modal analysis are then processed in a number of ways which are not available in commercial packages to give substantial gains in efficiency. First, a significant amount of pre- and post-processing of the system mass, stiffness and modal matrices can be performed to avoid much repetitive calculation. This is especially true for distributed excitation such as "rain-on-the-roof". Secondly, frequency averaging can be performed efficiently in a number of ways, as discussed in Section 3. This section also includes approximate expressions for the broadband average behaviour of a lightly damped system, which circumvents the need for any numerical frequency averaging.

An alternative to the global approach, and one which decreases the size of the numerical analysis significantly, is to perform individual FEA for each subsystem and couple these analyses together. Such an approach, using component-mode synthesis (CMS), is described in Section 4 and fits well with the SEA philosophy of coupled subsystem modes. The method is an extension of the global approach of Section 2. A numerical example is considered in Section 5.

The current paper concerns only cases where the damping in the system can be described in terms of a loss factor associated with each global mode, i.e., when the damping is proportional. The method can be extended straightforwardly for arbitrary spatial distributions of damping by allowing complex modal properties: this is not discussed here.

2. GLOBAL FINITE ELEMENT ANALYSIS AND ENERGY FLOW MODELS

This section concerns how the results of a global FEA can be used to form energy flow models. The system is assumed to be divided into two or more subsystems. Here it is assumed that subsystem a is excited. Expressions are developed for the input power, the total kinetic and potential energies in the system, the power dissipated and the kinetic and potential energy in subsystem b and the coupling powers for subsystem b.

The steps involved are briefly as follows. First the system is discretized and mass and stiffness matrices determined for each subsystem and for the system as a whole. Expressions for response quantities (energies, powers, etc.) are developed in terms of nodal responses. The second step is to determine the response to distributed time harmonic excitation. This is achieved by decomposing the response into global modes of vibration to make further calculations more efficient. The third step is to determine the response to particular forms of excitation, and, in particular, spatially uncorrelated excitation such as "rain-on-the-roof". The response to broadband excitation is found in Section 3.

2.1. FINITE ELEMENT DISCRETIZATION

The structure is discretized and the mass and stiffness matrices $\mathbf{M}$ and $\mathbf{K}$ determined. The response of the undamped system is then described by

$$\mathbf{M}\ddot{\mathbf{u}} + \mathbf{K}\mathbf{u} = \mathbf{f}^u, \tag{1}$$

where $\mathbf{u}$ is a vector of nodal degrees of freedom and $\mathbf{f}^u$ is a vector of corresponding nodal forces. (A list of symbols is given in Appendix C.) At the same time, the mass and stiffness matrices $\mathbf{M}_b$ and $\mathbf{K}_b$ are found for subsystem b. The nodal co-ordinates $\mathbf{u}_b$ for subsystem b are a subset of the global co-ordinates $\mathbf{u}$ and are related to them by

$$\mathbf{u}_b = \mathbf{S}_b\mathbf{u}, \tag{2}$$

where $\mathbf{S}_b$ is a transformation matrix. Some of the global co-ordinates $\mathbf{u}$ lie in only one subsystem, some lie in two or more (and hence represent coupling co-ordinates) and, possibly, some in no subsystem, these being associated only with coupling degrees of freedom. If the response is known, the potential and kinetic energies of the whole system and of subsystem b follow from

$$V = \tfrac{1}{2}\mathbf{u}^{\mathrm{T}}\mathbf{K}\mathbf{u}; \quad T = \tfrac{1}{2}\dot{\mathbf{u}}^{\mathrm{T}}\mathbf{M}\dot{\mathbf{u}}; \quad V_b = \tfrac{1}{2}\mathbf{u}_b^{\mathrm{T}}\mathbf{K}_b\mathbf{u}_b; \quad T_b = \tfrac{1}{2}\dot{\mathbf{u}}_b^{\mathrm{T}}\mathbf{M}_b\dot{\mathbf{u}}_b \tag{3}$$

where the superscript T denotes the transpose.

2.2. RESPONSE TO TIME HARMONIC EXCITATION: MODAL DECOMPOSITION

It is now assumed that the excitation is time harmonic, so that $\mathbf{f}^u = \mathbf{F}^u \exp(\mathrm{i}\omega t)$, $\mathbf{F}^u$ being a vector of force amplitudes. (In this paper the upper-case letter will be used to denote the complex amplitude of a time harmonic variable represented by the lower-case letter, and the time dependence will generally be suppressed.) Damping is allowed by introducing a loss factor η, assumed constant across the system. The response is then given by

$$\mathbf{U} = [\mathbf{K}(1 + \mathrm{i}\eta) - \omega^2\mathbf{M}]^{-1}\mathbf{F}^u. \tag{4}$$

The time-averaged total potential and kinetic energies become

$$V = \tfrac{1}{2}\mathrm{Re}\{\tfrac{1}{2}\mathbf{U}^{\mathrm{H}}\mathbf{K}\mathbf{U}\} = \tfrac{1}{4}\mathbf{U}^{\mathrm{H}}\mathbf{K}\mathbf{U}; \quad T = \tfrac{1}{2}\mathrm{Re}\{\tfrac{1}{2}(\mathrm{i}\omega\mathbf{U})^{\mathrm{H}}\mathbf{M}(\mathrm{i}\omega\mathbf{U})\} = \tfrac{1}{4}\omega^2\mathbf{U}^{\mathrm{H}}\mathbf{M}\mathbf{U}, \tag{5}$$

where H denotes the complex conjugate, or Hermitian transpose and $\mathrm{Re}\{\cdot\}$ denotes the real part. Similar expressions hold for the subsystem energies while the time-averaged input and coupling powers and the power dissipated in subsystem b are

$$P_{in} = \tfrac{1}{2}\mathrm{Re}\{\mathrm{i}\omega\mathbf{F}^{\mathrm{H}}\mathbf{U}\}; \quad P_{ab} = \tfrac{1}{2}\mathrm{Re}\{\mathrm{i}\omega\mathbf{F}_{ab}^{\mathrm{H}}\mathbf{U}_{ab}\}; \quad P_{diss,b} = \tfrac{1}{2}\omega\eta\,\mathbf{U}_b^{\mathrm{H}}\mathbf{K}_b\mathbf{U}_b = 2\omega\eta V_b, \tag{6}$$

where $\mathbf{F}_{ab}$ and $\mathbf{U}_{ab}$ are the internal forces and displacements at the coupling co-ordinates between subsystems a and b. In practice, it is perhaps easier to find the coupling power from conservation of energy considerations, especially if a coupling co-ordinate is common to three or more subsystems, when the coupling powers are not defined uniquely [12].

Although it is quite possible to calculate the response using equations (4)–(6), it is very time-consuming to perform the matrix inversion of equation (4) at each frequency. It is numerically more efficient to proceed by modal decomposition, using the global modes of the whole system. While there are as many such modes as there are nodal co-ordinates, the contributions of many of the modes can often be neglected.

A modal analysis yields the natural frequencies ω_j and mode shapes $\boldsymbol{\phi}_j$ for $j = 1, \ldots, m$, where m is the number of retained modes. The mode shapes are assumed to be mass normalized, so that the orthogonality conditions are

$$\mathbf{P}^{\mathrm{T}}\mathbf{M}\mathbf{P} = \mathbf{I}; \quad \mathbf{P}^{\mathrm{T}}\mathbf{K}\mathbf{P} = \mathrm{diag}(\omega_j^2); \quad \mathbf{P} = [\boldsymbol{\phi}_1 \quad \boldsymbol{\phi}_2 \quad \cdots \quad \boldsymbol{\phi}_m], \tag{7}$$

where $\mathbf{P}$ is the modal matrix, whose columns are the mode shapes, and $\mathrm{diag}(\cdot)$ indicates a diagonal matrix. The modal forces F_j^y and the response Y_j of the jth mode are then

$$F_j^y = \boldsymbol{\phi}_j^{\mathrm{T}}\mathbf{F}^u, \quad Y_j = \alpha_j F_j^y; \quad j = 1, \ldots, m, \tag{8}$$

where the modal receptance is given by

$$\alpha_j = \frac{1}{\omega_j^2(1 + \mathrm{i}\eta) - \omega^2} \tag{9}$$

and where the response, equation (4), becomes $\mathbf{U} = \mathbf{P}\mathbf{Y}$, $\mathbf{Y}$ being the vector of modal responses. The total system time-averaged potential and kinetic energies become

$$V = \frac{1}{4}\sum_j \omega_j^2 |Y_j|^2; \qquad T = \frac{1}{4}\omega^2 \sum_j |Y_j|^2 \tag{10}$$

and are simply the sums of the individual energies associated with each of the modes. The expressions for the subsystem energies are more complicated, since the mode shapes are orthogonal over the whole system and not over the individual subsystems. For subsystem b, they are given by

$$V_b = \tfrac{1}{4}\mathbf{Y}^{\mathrm{H}}\boldsymbol{\kappa}_b\mathbf{Y}; \qquad T_b = \tfrac{1}{4}\omega^2\mathbf{Y}^{\mathrm{H}}\boldsymbol{\mu}_b\mathbf{Y} \tag{11}$$

where the matrices

$$\boldsymbol{\kappa}_b = \mathbf{P}^{\mathrm{T}}\mathbf{S}_b^{\mathrm{T}}\mathbf{K}_b\mathbf{S}_b\mathbf{P}; \qquad \boldsymbol{\mu}_b = \mathbf{P}^{\mathrm{T}}\mathbf{S}_b^{\mathrm{T}}\mathbf{M}_b\mathbf{S}_b\mathbf{P} \tag{12}$$

are real, symmetric and generally full. These expressions are here termed the stiffness and mass distribution matrices of subsystem b, and represent the stiffness and mass of subsystem b expressed in global modal co-ordinates.

2.3. COMPUTATIONAL CONSIDERATIONS

While equation (11) can be used to calculate the response in subsystem b, substantial computational benefits can be made by rearranging this expression. Equation (11) can be written as a sum of cross-modal terms involving global modes m and p, so, for example,

$$V_b = \frac{1}{4} \sum_{m,p} Y_m^* Y_p \kappa_{b,mp} \tag{13}$$

while the modal response is

$$Y_p = \alpha_p F_p^y = \alpha_p \sum_k P_{kp} F_k^u, \tag{14}$$

where the summation runs over all excited nodes. Substitution and reordering the two summations gives

$$V_b = \frac{1}{4} \sum_{m,p} \psi_{a,mp} \kappa_{b,mp} \alpha_m^* \alpha_p, \tag{15}$$

where the expression

$$\psi_{a,mp} = \sum_{j,k} P_{jm} P_{kp} F_j^{u^*} F_k^u \tag{16}$$

is termed the (m, p)th force distribution term associated with subsystem a. The force distribution matrix of subsystem a, $\boldsymbol{\psi}_a$, determines the applied excitation in global modal co-ordinates and is given by

$$\boldsymbol{\psi}_a = \mathbf{P}^{\mathrm{T}} \mathbf{S}_a^{\mathrm{T}} \mathbf{A} \mathbf{S}_a \mathbf{P}; \qquad A_{jk} = F_j^{u^*} F_k^u, \tag{17}$$

where $\mathbf{A}$ depends on the magnitudes and phases of the various nodal forces. Gains in computational efficiency arise because the terms $\psi_{a,mp}$ and $\kappa_{b,mp}$ and their product need only be evaluated once.

2.4. SPATIALLY DISTRIBUTED EXCITATION AND RAIN-ON-THE-ROOF

Often the spatial distribution of the excitation is frequency independent, although the absolute levels may not be. Under this circumstances the force distribution matrix $\boldsymbol{\psi}_a$ need only be evaluated once, leading to substantial reductions in computational effort. In this section, different forms of excitation are discussed with particular reference to the case of rain-on-the-roof excitation, where further simplifications are possible.

2.4.1. *Spatially distributed coherent excitation*

The excitation may be broadband but coherent. In general, $\mathbf{A}$ and $\boldsymbol{\psi}_a$ are full, complex and Hermitian. (If, however, the phase of the excitation is constant across the subsystem then the subsystem force distribution matrix becomes real.) The total potential and kinetic

energies and input power to subsystem a are given by

$$V = \frac{1}{4}\sum_m \psi_{a,mm}\omega_m^2|\alpha_m|^2; \quad T = \frac{1}{4}\omega^2\sum_m \psi_{a,mm}|\alpha_m|^2; \quad P_{in} = \frac{1}{2}\mathrm{Re}\left\{\mathrm{i}\omega\sum_m \psi_{a,mm}\alpha_m\right\}, \tag{18}$$

The force distribution term $\psi_{a,mm}$ indicates how well the mth global mode is excited and depends on the mode shape within the excited subsystem and the force distribution. The potential and kinetic energies in subsystem b are given by

$$V_b = \sum_{m,p}(\psi_{a,mp}\kappa_{b,mp})\Gamma_{mp}; \quad T_b = \sum_{m,p}(\psi_{a,mp}\mu_{b,mp})\omega^2\Gamma_{mp}, \tag{19}$$

where the term Γ_{mp} is frequency dependent and is given by

$$\Gamma_{mp} = \tfrac{1}{4}\alpha_m^*\alpha_p. \tag{20}$$

The response in subsystem b depends not only on how well the global modes are excited (through the force distribution terms) but also how strongly these modes respond in subsystem b. Computational gains arise because the terms in parentheses in equation (19) need only be evaluated once.

2.4.2. *Spatially distributed incoherent excitation*: *rain-on-the roof*

Suppose now that the excitation is broadband but incoherent, in that it is spatially delta-correlated. (Equivalently, one might consider the case where the excitation is coherent, but the relative phase between excitations applied at different locations is unknown, or the case of predicting the expected response to a point force applied at some unknown location). Under these circumstances, the energy response can be found by summing the energy response due to excitation applied to each point in the excited subsystem.

One particular excitation, rain-on-the-roof, is of particular interest. This is defined here as spatially delta-correlated, broadband excitation whose magnitude at any location is proportional to the local mass density. Such excitation excites the local modes of the excited subsystem equally (i.e., it inputs power equally into all modes). When the structure is then discretized to form the FE model, then it can be shown (Appendix A) that the matrix $\mathbf{A}$ is real and proportional to the mass matrix of the excited subsystem, $\mathbf{M}_a$, if a consistent formulation is adopted in deriving the nodal forces. The constant of proportionality then indicates the level of excitation and $\boldsymbol{\psi}_a$ then equals the subsystem mass distribution matrix $\boldsymbol{\mu}_a$.

Again, it should be noted that the terms in parentheses in equation (19) need only be evaluated once, and only the vector $\boldsymbol{\alpha}$ needs to be calculated at different frequencies.

3. FREQUENCY AVERAGES

Most applications of energy flow methods involve random broadband excitation and interest lies in frequency-averaged response quantities. In most cases, furthermore, the spatial distribution of the excitation is independent of frequency, while the level of excitation may not be. Under this circumstances, the terms A_{jk} are related to the power- and cross-spectral densities of the nodal forces so that $\boldsymbol{\psi}_a$ can be written as

$$\boldsymbol{\psi}_a(\omega) = R^2(\omega)\boldsymbol{\psi}'_a, \tag{21}$$

where $\boldsymbol{\psi}'_a$ is found by putting some reference nodal force equal to unity and where $R^2(\omega)$ represents the frequency variation. For the particular case of rain, for example, $\mathbf{A} = \mathbf{M}_a$ and $\boldsymbol{\psi}'_a = \boldsymbol{\mu}_a$. The excitation has a power-spectral density S_{ff} such that $R^2(\omega) = S_{ff}(\omega)\delta\omega$ in a frequency band $\delta\omega$. The frequency-averaged response is then found by averaging equations (18) and (19) over the frequency band of interest. Note, however, that only the terms, α, ω and perhaps S_{ff} are frequency dependent, so that the summation and the frequency integration can be performed independently, resulting in much reduced computation time. For example, over a frequency band Ω of bandwidth B

$$\bar{T}_b = \frac{1}{4B} \sum_{m,p} (\psi'_{a,mp} \mu_{b,mp}) \left(\int_\Omega S_{ff} \omega^2 \alpha^*_m \alpha_p \, \mathrm{d}\omega \right). \tag{22}$$

Equations (18) and (19) can be integrated numerically. However, if S_{ff} and η are constant (and perhaps also if they are known functions of frequency) then the frequency integrals can be evaluated analytically. This yields further substantial gains in numerical efficiency. In practice, if η is a function of frequency, but the damping is light such that $\eta^2 \ll 1$, then negligible errors are introduced by replacing $\eta(\omega)$ with $\eta_j = \eta(\omega_j)$ in $\alpha_j(\omega)$. Under these circumstances the frequency averages become

$$\bar{V} = \left(\frac{S_{ff}}{4B}\right) \sum_m \omega_m^2 \psi'_{a,mm} J_{1,m}, \quad J_{1,m} = \int_\Omega |\alpha_m|^2 \, \mathrm{d}\omega,$$

$$\bar{T} = \left(\frac{S_{ff}}{4B}\right) \sum_m \psi'_{a,mm} J_{2,m}, \quad J_{2,m} = \int_\Omega \omega^2 |\alpha_m|^2 \, \mathrm{d}\omega,$$

$$\bar{P}_{in} = \left(\frac{S_{ff}}{2B}\right) \sum_m \psi'_{a,mm} J_{3,m}, \quad J_{3,m} = \int_\Omega \mathrm{Re}\{\mathrm{i}\omega\alpha_m\} \, \mathrm{d}\omega,$$

$$\bar{V}_b = \left(\frac{S_{ff}}{4B}\right) \sum_{m,p} \psi'_{a,mp} \kappa_{b,mp} J_{4,mp}, \quad J_{4,mp} = \int_\Omega \alpha^*_m \alpha_p \, \mathrm{d}\omega,$$

$$\bar{T}_b = \left(\frac{S_{ff}}{4B}\right) \sum_{m,p} \psi'_{a,mp} \mu_{b,mp} J_{5,mp}, \quad J_{5,mp} = \int_\Omega \omega^2 \alpha^*_m \alpha_p \, \mathrm{d}\omega. \tag{23}$$

The frequency integrals J are all integrable in closed form, the expressions being given in Appendix B. The terms $J_{1,i}$, $J_{2,i}$ and $J_{3,i}$ are generally small except for the modes i which are resonant, i.e., if ω lies in Ω. The cross-mode coupling terms $J_{4,ij}$ and $J_{5,ij}$ are generally small except for those mode pairs which overlap, i.e., whose natural frequencies are close, their separation being less than the modal half-power bandwidths, and which are resonant. Therefore, computational savings can be made by limiting the cross-modal summations to modes within and close to the frequency band of interest, although care should be taken if there are relatively few resonant modes in Ω, since non-resonant modes may contribute significantly to the infinite sums.

3.1. SMALL DAMPING APPROXIMATIONS

If the damping is light such that $\eta^2 \ll 1$, then $\alpha_j(\omega)$ and the integrands of equation (23) are dominated by sharp resonances around the corresponding natural frequencies ω_j. For

modes which are resonant in Ω the integrals are well approximated by replacing the frequency range of integration by $(0, \infty)$ (e.g., reference [13]), in which case

$$J_{1,j} \approx \frac{\pi}{2\eta_j \omega_j^3}, \quad J_{2,j} \approx \frac{\pi}{2\eta_j \omega_j}, \quad J_{3,j} \approx \frac{\pi}{2}; \quad \omega_j \in \Omega. \tag{24}$$

For non-resonant modes (i.e, those for which $\omega_j \notin \Omega$) the integrals are approximately zero, these modes contributing very little to the total response. Similarly, the integrals $J_{4,ij}$ and $J_{5,ij}$ are approximated by

$$\left.\begin{aligned} J_{4,ij} &\approx \frac{\pi(\omega_i + \omega_j)^2[\eta_i(2\omega_i - \omega_j) + \eta_j(2\omega_j - \omega_i)]}{4\omega_i\omega_j[(\omega_i^2 - \omega_j^2)^2 + (\eta_i\omega_j^2 + \eta_j\omega_j^2)^2]} \\ J_{5,ij} &\approx \frac{\pi(\omega_i + \omega_j)^2[\eta_i\omega_i + \eta_j\omega_j]}{4[(\omega_i^2 - \omega_j^2)^2 + (\eta_i\omega_i^2 + \eta_j\omega_j^2)^2]} \end{aligned}\right\} \quad \omega_i, \omega_j \in \Omega. \tag{25}$$

Note that these cross-modal terms are large if the modal separation $|\omega_i - \omega_j|$ is smaller than the average modal bandwidth $\Delta = (\eta_i\omega_i + \eta_j\omega_j)/2$, that is, if the modes overlap. The terms $\kappa_{b,ij}$ and $\mu_{b,ij}$ then indicate the degree to which the (i, j)th modal pair contributes to the potential and kinetic energies in the bth subsystem. Note also that there is a clear similarity between these expressions (particularly the denominators) and those that define the coupling power between two coupled oscillators [1], the difference being that here the coupling occurs between two global modes of vibration rather than two modes of the uncoupled system.

Thus, the response quantities reduce to a sum of contributing modal terms. The input power and total energies depend on the total number of modes in the frequency band of excitation, while the subsystem energies depend not only on the total number of modes in Ω but also on the modal overlap, i.e., how many cross-modal terms contribute to J_4 and J_5.

4. LOCAL FINITE ELEMENT ANALYSIS AND ENERGY FLOW MODELS

Rather than describing the response of the system in terms of a large number of nodal degrees of freedom, it is computationally more efficient to describe the response in terms of the component modal responses of each subsystem. This forms the basis of component-mode synthesis (CMS) [14]. The component modes may be found by performing a finite element analysis for each subsystem in turn, thus solving a number of smaller problems rather than one large one. A CMS model is particularly well suited for postprocessing into an energy flow model, since the global degrees of freedom of the structure are easily partitioned into subsystem degrees of freedom. In the following section expressions for the system response using a fixed interface CMS approach [15] are derived. The expressions are identical to those derived previously with the terms ψ, κ and μ now being given in terms of component modal co-ordinates.

4.1. THE EQUATIONS OF MOTION

Four different sets of co-ordinates are used to describe the response of the structure: nodal, uncoupled component modal, coupled component modal and global modal degrees of freedom. The structure is split into n subsystems and a finite element model of each subsystem is generated. The nodal degrees of freedom are contained in a vector $\mathbf{u}$, which is

partitioned into the degrees of freedom associated with each subsystem, so that

$$\mathbf{u} = [\mathbf{u}_1^{\mathrm{T}} \quad \mathbf{u}_2^{\mathrm{T}} \quad \cdots \quad \mathbf{u}_n^{\mathrm{T}}]^{\mathrm{T}}. \tag{26}$$

Each subvector in equation (26) is further partitioned into interior and coupling degrees of freedom, so that, for example, the degrees of freedom associated with the rth subsystem are given by

$$\mathbf{u}_r = [\mathbf{u}_i^{\mathrm{T}} \ \mathbf{u}_c^{\mathrm{T}}]_r^{\mathrm{T}}. \tag{27}$$

The coupling degrees of freedom are degrees of freedom which are common to two or more subsystems. The undamped equations of motion for the uncoupled structure can be written as

$$\mathbf{m}^u\ddot{\mathbf{u}} + \mathbf{k}^u\mathbf{u} = \mathbf{f}^u, \tag{28}$$

where $\mathbf{m}^u$ and $\mathbf{k}^u$ are block-diagonal, the rth submatrices on the diagonals being given by

$$\mathbf{m}_r^u = \begin{bmatrix} \mathbf{m}_{ii} & \mathbf{m}_{ic} \\ \mathbf{m}_{ci} & \mathbf{m}_{cc} \end{bmatrix}_r; \qquad \mathbf{k}_r^u = \begin{bmatrix} \mathbf{k}_{ii} & \mathbf{k}_{ic} \\ \mathbf{k}_{ci} & \mathbf{k}_{cc} \end{bmatrix}_r \tag{29}$$

while the rth subvector associated with $\mathbf{f}^u$ is given by

$$\mathbf{f}_r^u = \begin{bmatrix} \mathbf{f}_i \\ \mathbf{f}_c \end{bmatrix}_r. \tag{30}$$

A local modal analysis of each subsystem is then performed with the coupling degrees of freedom associated with each subsystem being fully constrained. The nodal degrees of freedom $\mathbf{u}$, are related to a set of uncoupled component modal degrees of freedom $\mathbf{q}$, by the transformation

$$\mathbf{u} = \mathbf{T}\mathbf{q}, \tag{31}$$

where the rth submatrix on the diagonal of $\mathbf{T}$ is given by

$$\mathbf{T}_r = \begin{bmatrix} \mathbf{P}_r^q & \boldsymbol{\chi}_r \\ 0 & \mathbf{I} \end{bmatrix} \tag{32}$$

and where $\mathbf{P}_r^q$ is a matrix of the local mode shapes and $\boldsymbol{\chi}_r$ is a matrix of constraint modes given by

$$\boldsymbol{\chi}_r = -\mathbf{k}_{ii,r}^{u\ -1}\mathbf{k}_{ic,r}^u; \quad \mathbf{P}_r^{q,\mathrm{T}}\mathbf{k}_{ii,r}^u\mathbf{P}_r^q = \omega_{n,r}^2; \quad \mathbf{P}_r^{q,\mathrm{T}}\mathbf{m}_{ii,r}^u\mathbf{P}_r^q = \mathbf{I}. \tag{33}$$

The constraint modes give the shape of the subsystem when a particular coupling degree of freedom is given a unit displacement or rotation, whilst all other coupling degrees of freedom remain fixed. A fundamental assumption of CMS is that there are fewer component modal degrees of freedom than nodal degrees of freedom. The uncoupled component modal mass and stiffness matrices are given by

$$\mathbf{m}^q = \mathbf{T}^{\mathrm{T}}\mathbf{m}^u\mathbf{T}; \quad \mathbf{k}^q = \mathbf{T}^{\mathrm{T}}\mathbf{k}^u\mathbf{T}, \tag{34}$$

where the rth submatrices on the respective diagonals of $\mathbf{m}^q$ and $\mathbf{k}^q$ are given by

$$\mathbf{m}_r^q = \mathbf{T}_r^{\mathrm{T}}\mathbf{m}_r^u\mathbf{T}_r; \quad \mathbf{k}_r^q = \mathbf{T}_r^{\mathrm{T}}\mathbf{k}_r^u\mathbf{T}_r. \tag{35}$$

The local finite element models are then coupled together by enforcing continuity between the various coupling degrees of freedom. The global response of the structure is then described by the set of coupled component modal co-ordinates $\mathbf{x}$. The uncoupled component modal co-ordinates can be related to these by a transformation matrix $\boldsymbol{\beta}$, such that

$$\mathbf{q} = \boldsymbol{\beta}\mathbf{x}. \tag{36}$$

The uncoupled component modal co-ordinates associated with the rth subsystem are related to the set of coupled component mode co-ordinates using the appropriate partition of $\boldsymbol{\beta}$

$$\mathbf{q}_r = \boldsymbol{\beta}_r \mathbf{x}. \tag{37}$$

The undamped global equations of motion are then given by

$$\mathbf{m}^x \ddot{\mathbf{x}} + \mathbf{k}^x \mathbf{x} = \mathbf{f}^x, \tag{38}$$

where the global mass and stiffness matrices and the global force vector are given by

$$\mathbf{m}^x = \boldsymbol{\beta}^{\mathrm{T}} \mathbf{m}^q \boldsymbol{\beta}; \quad \mathbf{k}^x = \boldsymbol{\beta}^{\mathrm{T}} \mathbf{k}^q \boldsymbol{\beta}; \quad \mathbf{f}^x = \boldsymbol{\beta}^{\mathrm{T}} \mathbf{f}^q. \tag{39}$$

4.2. CALCULATING THE RESPONSE: GLOBAL MODAL DECOMPOSITION

Following Section 2.2, if the excitation is time harmonic then the time-averaged response quantities can be written in terms of the uncoupled component-mode co-ordinates as

$$V_b = \tfrac{1}{4}\mathbf{Q}_b^{\mathrm{H}} \mathbf{k}_b^q \mathbf{Q}_b; \quad T_b = \tfrac{1}{4}\omega^2 \mathbf{Q}_b^{\mathrm{H}} \mathbf{m}_b^q \mathbf{Q}_b; \quad P_{in} = \tfrac{1}{2}\mathrm{Re}\{\mathrm{i}\omega \mathbf{F}_a^{q,\mathrm{H}} \mathbf{Q}_a\}. \tag{40}$$

Equation (38) could be solved by matrix inversion. For example, the uncoupled component-mode response in subsystem b is given by

$$\mathbf{Q}_b = \boldsymbol{\beta}_b [\mathbf{k}^x (1 + \mathrm{i}\eta) - \omega^2 \mathbf{m}^x]^{-1} \mathbf{F}^x. \tag{41}$$

However, such an approach is still computationally expensive, even though the global mass and stiffness matrices are now much smaller than in the global FEA of Section 2. A more efficient procedure is to again perform a global modal analysis. This yields the global natural frequencies ω_j and global mode shapes $\boldsymbol{\phi}_j$ for $j = 1, \ldots, m$. The global modes are assumed to be mass normalized so that

$$\mathbf{P}^{\mathrm{T}} \mathbf{m}^x \mathbf{P} = \mathbf{I}; \quad \mathbf{P}^{\mathrm{T}} \mathbf{k}^x \mathbf{P} = \mathrm{diag}(\omega_j^2); \quad \mathbf{P} = [\boldsymbol{\phi}_1 \quad \boldsymbol{\phi}_2 \quad \cdots \quad \boldsymbol{\phi}_m] \tag{42}$$

using the same notation for the global modal degrees of freedom and modal receptances as in Section 2. The uncoupled component-mode response in subsystem b is then given by

$$\mathbf{Q}_b = \boldsymbol{\beta}_b \mathbf{P} \mathrm{diag}(\alpha_j) \mathbf{P}^{\mathrm{T}} \mathbf{F}^x. \tag{43}$$

The stiffness and mass distribution matrices associated with subsystem b are therefore given by

$$\boldsymbol{\kappa}_b = \mathbf{P}^{\mathrm{T}} \boldsymbol{\beta}_b^{\mathrm{T}} \mathbf{k}_b^q \boldsymbol{\beta}_b \mathbf{P}; \quad \boldsymbol{\mu}_b = \mathbf{P}^{\mathrm{T}} \boldsymbol{\beta}_b^T \mathbf{m}_b^q \boldsymbol{\beta}_b \mathbf{P}. \tag{44}$$

Since there are significantly fewer component modal degrees of freedom than nodal degrees of freedom, equation (44) requires substantially less computation than equation (13).

4.3. COMPUTATIONAL CONSIDERATIONS

The issues discussed in Sections 2.3, 2.4 and 3 regarding efficient computation apply equally here. The potential energy can be written as

$$V_b = \frac{1}{4} \sum_{m,p} Y_m^* Y_p \kappa_{b,mp}. \tag{45}$$

Using the transformation matrices, the global modal response can be written in terms of the local nodal forces as

$$Y_p = \alpha_p F_p^y = \alpha_p \sum_j P_{jp} F_j^x = \alpha_p \sum_j P_{jp} \sum_k \beta_{kj} F_k^q = \alpha_p \sum_j P_{jp} \sum_k \beta_{kj} \sum_l T_{lk} F_l^u, \tag{46}$$

where j runs over all coupled component modes, k runs over all uncoupled component modes and l runs over all excited nodes. Substituting into equation (45) and reordering gives

$$V_b = \frac{1}{4} \sum_{m,p} \alpha_m^* \alpha_p \kappa_{b,mp} \sum_{j,r} P_{jm} P_{rp} \sum_{k,s} \beta_{kj} \beta_{sr} \sum_{l,t} T_{lk} T_{ts} F_l^{u^*} F_t^u. \tag{47}$$

The nodal force distribution matrix is defined by

$$\mathbf{A}_{lt}^u = F_l^{u^*} F_t^u \tag{48}$$

and the subsystem kinetic and potential energies can then be written as

$$V_b = \frac{1}{4} \sum_{m,p} \psi_{a,mp} \kappa_{b,mp} \alpha_m^* \alpha_p; \qquad T_b = \frac{1}{4} \omega^2 \sum_{m,p} \psi_{a,mp} \mu_{b,mp} \alpha_m^* \alpha_p, \tag{49}$$

where the global force distribution matrix is given by

$$\boldsymbol{\psi}_a = \mathbf{P}^{\mathrm{T}} \boldsymbol{\beta}_a^{\mathrm{T}} \mathbf{T}_a^{\mathrm{T}} \mathbf{A}_a^u \mathbf{T}_a \boldsymbol{\beta}_a \mathbf{P}. \tag{50}$$

The input power is given by

$$P_{in} = \frac{1}{2} \mathrm{Re} \left\{ \mathrm{i}\omega \sum_m \psi_{a,mm} \alpha_m \right\}. \tag{51}$$

For arbitrary force distributions, $\boldsymbol{\psi}_a$ (equation (50)) may be complex as discussed previously. For the case of rain-on-the-roof excitation, the nodal force distribution matrix $\mathbf{A}_a^u$ is real and proportional to the nodal mass matrix $\mathbf{m}_a^u$. Then $\boldsymbol{\psi}_a$ is equal to the mass distribution matrix $\boldsymbol{\mu}_a$ of equation (44). Frequency averages can also be found by integrating only those frequency-dependent terms, as described in Section 3.

5. NUMERICAL EXAMPLE

The use of the previous expressions is demonstrated by considering the response of the plate structure shown in Figure 1. Three plates are joined together in a corner configuration with each plate representing a subsystem. The properties and dimensions of the structure

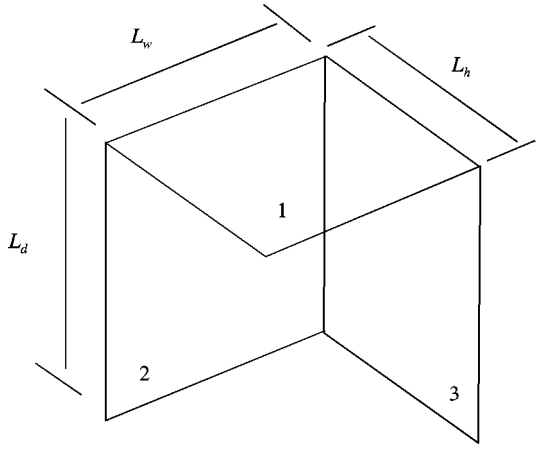

Figure 1. Three-plate structure.

TABLE 1

Structural properties

Young's modulus	210 GN/m^2
Density	7800 kg/m^3
Poisson's ratio	0·3
Loss factor	0·01
Thickness	0·001 m
L_w	0·255 m
L_h	0·225 m
L_d	0·275 m

are shown in Table 1. The energy associated with rigid-body motion is neglected. Furthermore, in the frequency range of interest here, in-plane motion can be neglected and the motion described purely in terms of bending vibrations. The modal densities of subsystems 1, 2 and 3 are respectively 18·3, 22·3 and 19·7 modes per kHz. The structure is modelled using a fixed interface component-mode synthesis approach. Each individual plate is modelled using 144 Heterosis plate elements [16] with additional degrees of freedom added to allow for in-plane displacements. The local eigenvalue problem is solved using subspace iteration to obtain 35 local modes per subsystem. The global mass and stiffness matrices are then assembled and the first 100 global modes obtained. While this procedure may be carried out by postprocessing the results from a commercial FE package, in this example the routines were implemented using Matlab. The component-mode synthesis approach reduces the size of the finite element calculations: if a global finite element analysis were performed the model would have over 8000 degrees of freedom; instead three finite element problems, each with 2693 degrees of freedom, are solved; in the global assembly 35 interior and 195 constraint degrees of freedom for each subsystem are retained and the resulting global analysis has 396 degrees of freedom.

In Figure 2 the asymptotic global mode count and the FE computed mode count (neglecting rigid-body modes) are compared. The mass and stiffness distribution matrices can be calculated using equation (44). These matrices only need to be evaluated once for

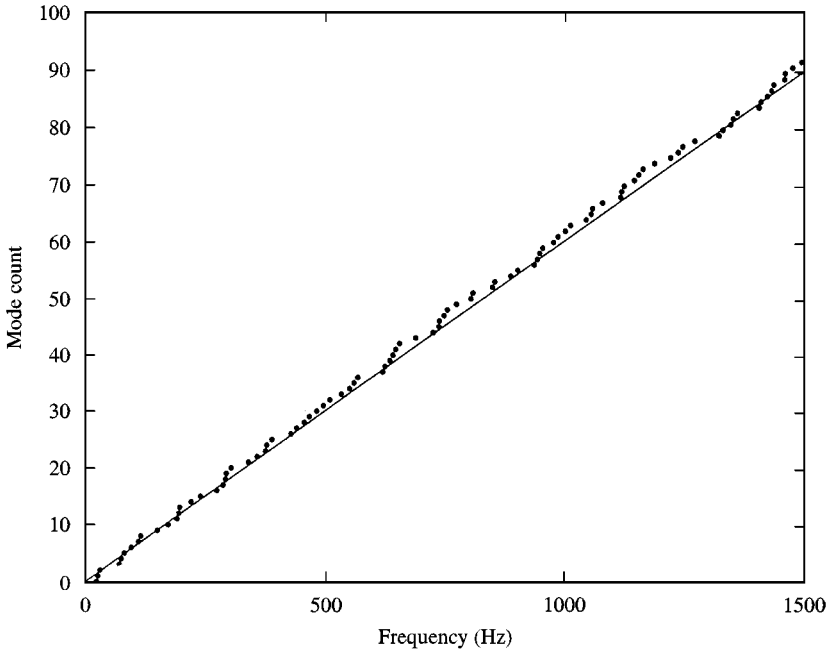

Figure 2. Mode count of three-plate structure: ——, asymptotic mode count; ●●●, FE computed mode count.

a given structure. Figure 3 shows the mass distribution terms associated with the first 30 global modes for the three subsystems (neglecting rigid-body modes). The diagonal terms indicate the proportions of the global modal masses associated with each subsystem. These typically vary substantially from the distribution of actual mass across the subsystems: these variations in the diagonal terms indicate that the global modes of the structure have a tendency to be localized to one or two subsystems rather than be spread uniformly across all three. As an example, Figure 4 shows the 22nd global mode, which is localized in the first and second subsystems. The off-diagonal mass distribution terms give an indication of the mass orthogonality of the global modes when evaluated over various subsystems.

The global modal receptances can be calculated for various discrete excitation frequencies. In this example, the response at each frequency is calculated using the first 100 global modes. The frequency terms in equation (19) can then be calculated. Figure 5 shows the magnitude of the frequency-dependent terms associated with the kinetic energy, $\omega^2 \Gamma_{ij}$, for the first 30 modes, due to excitation at a frequency of 300 Hz. At this frequency, the modal overlap is 0·18. Modes close to the excitation frequency have the largest response, whilst the cross-modal response decreases as the difference in mode number increases.

The potential and kinetic energies in subsystem b are then found by evaluating the appropriate scalar products of the matrices $\boldsymbol{\psi}_a$, $\boldsymbol{\kappa}_b$, $\boldsymbol{\mu}_b$, $\boldsymbol{\Gamma}$ and $\omega^2\boldsymbol{\Gamma}$ from equation (19). Similarly, the input power to subsystem a is found by evaluating equation (18). An energy influence coefficient A_{ba} can then be defined as the energy in the bth subsystem per unit input power applied to subsystem a. Figure 6 shows the matrix of energy influence coefficients (EICs) for the structure, calculated using the finite element approach, as a function of frequency for discrete excitation frequency. Also shown in Figure 6 are estimates of the EICs obtained using a traditional SEA model of the plate structure. The discrete frequency finite element response is seen to be distinctly resonant in nature.

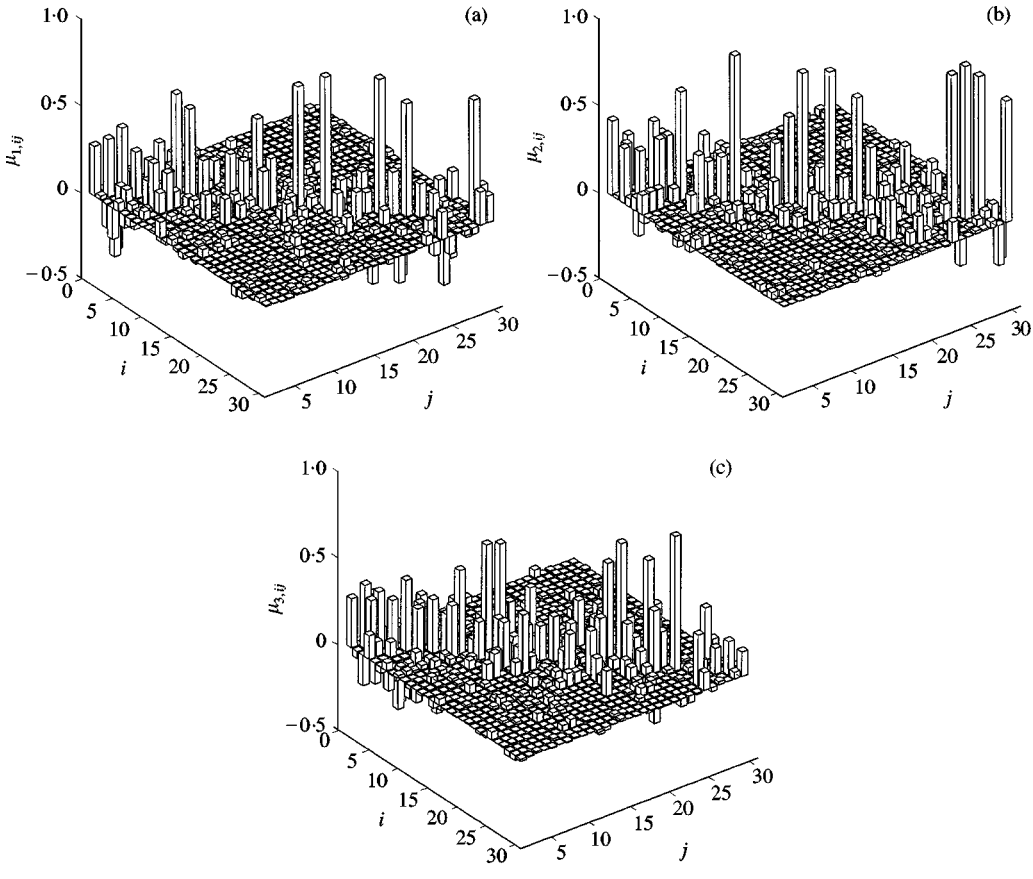

Figure 3. Elements of the subsystem mass distribution matrices for the three-plate system, lowest 30 global modes: (a) $\mu_{1,ij}$; (b) $\mu_{2,ij}$; (a) $\mu_{3,ij}$.

The frequency average response can be obtained using the analytical expressions for the integrals J_i given in Appendix A. As an example, the magnitudes of the first 30 rows and columns of the matrix $\mathbf{J}_5$ are shown in Figure 7, for excitation over a 100 Hz frequency band, with a centre frequency of 300 Hz. The 100 Hz frequency band contains around six global modes. The frequency average EICs are found by dividing the frequency average energy in subsystem i, by the frequency averaged input power applied to subsystem j. Figures 8 and 9 show frequency averaged EICs, found by frequency averaging over 100 and 200 Hz frequency bands respectively as functions of the centre frequency of the excitation. It can be seen that SEA tends to overpredict the response in the undriven subsystems. This is because, in this example, the subsystems are strongly coupled. For example, in the exact wave theories in references [17, 18], the strength of coupling is quantified in terms of a parameter γ, and the coupling is strong if $\gamma > 1$: here γ is approximately 8 at a frequency of 750 Hz.

6. CONCLUDING REMARKS

In this paper, computationally efficient methods of forming energy flow models from finite element analyses were described. These involved both global and local finite element

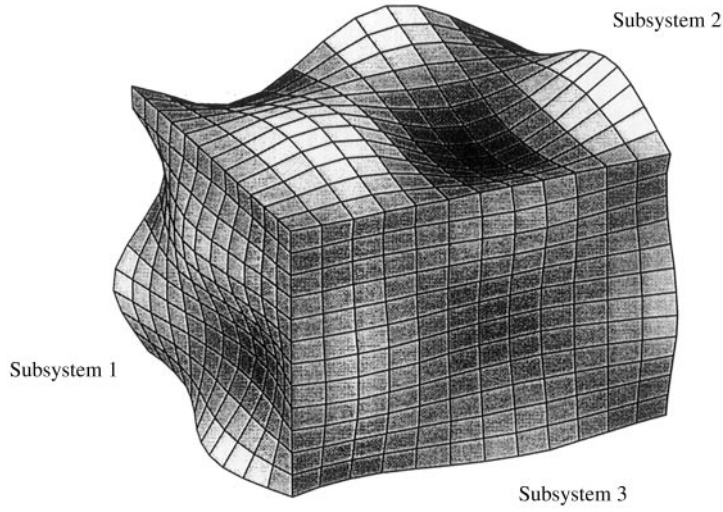

Figure 4. The 22nd global mode shape of the three-plate structure (note localization in subsystems 1 and 3).

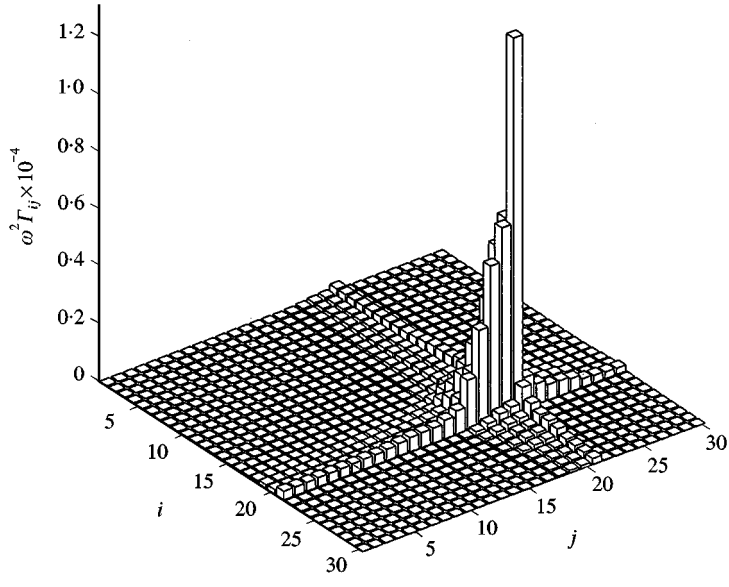

Figure 5. Frequency-dependent cross-modal terms $\omega^2\Gamma_{ij}$ for the three-plate system, lowest 30 global modes, excitation at 300 Hz.

models, the latter being based on component-mode synthesis. A global modal analysis is then performed, leading to responses which are expressed in terms of a sum of components which indicate the interaction of pairs of global modes.

The gains in numerical efficiency arise from four sources: first because the numerical operations involved in post-processing can be reordered in such a way that computationally expensive calculations normally need to be performed only once; secondly, because the terms which are frequency dependent (i.e, those involving the global modal receptances)

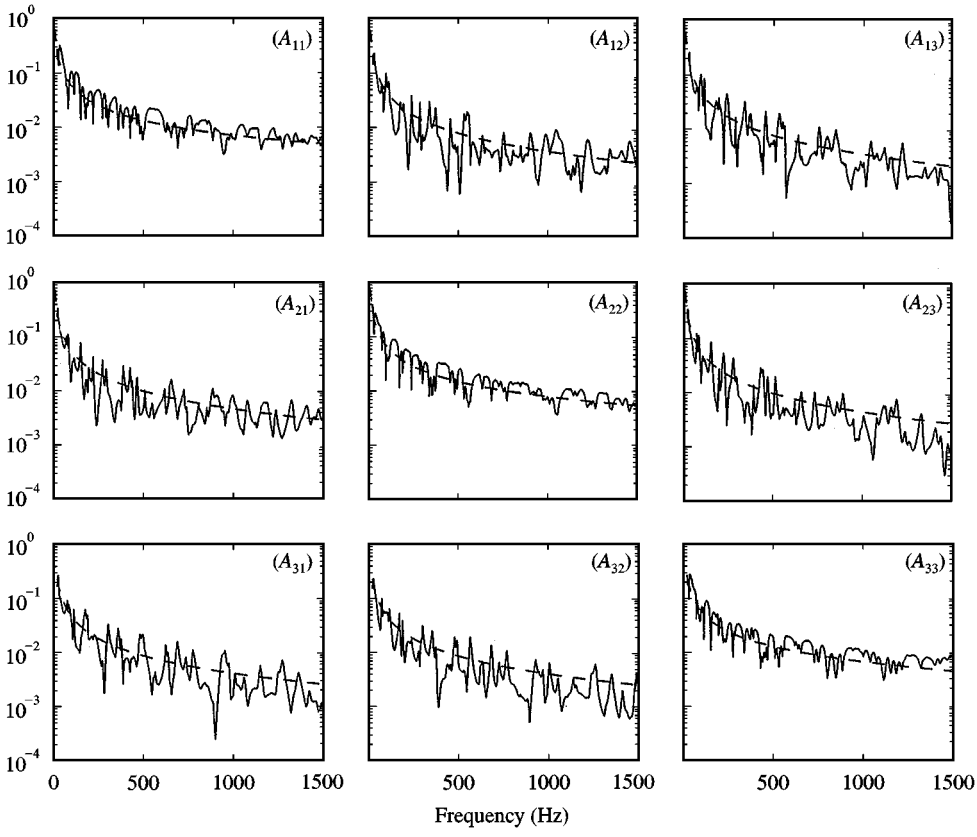

Figure 6. Energy influence coefficients A_{ij} for the three-plate system, discrete frequency excitation (i, j indicated in upper right-hand corners of figures); – – – SEA predictions.

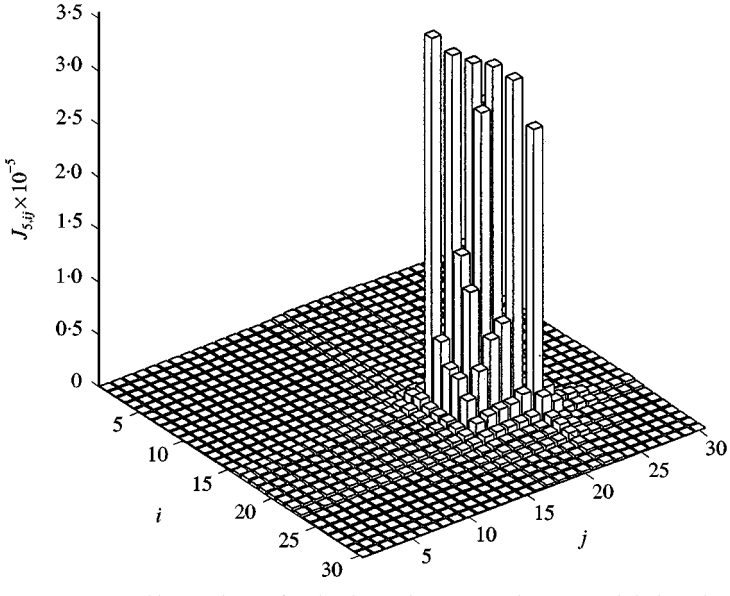

Figure 7. Frequency-averaged integrals $J_{5,ij}$ for the three-plate system, lowest 30 global modes, frequency band 100 Hz centred at 300 Hz.

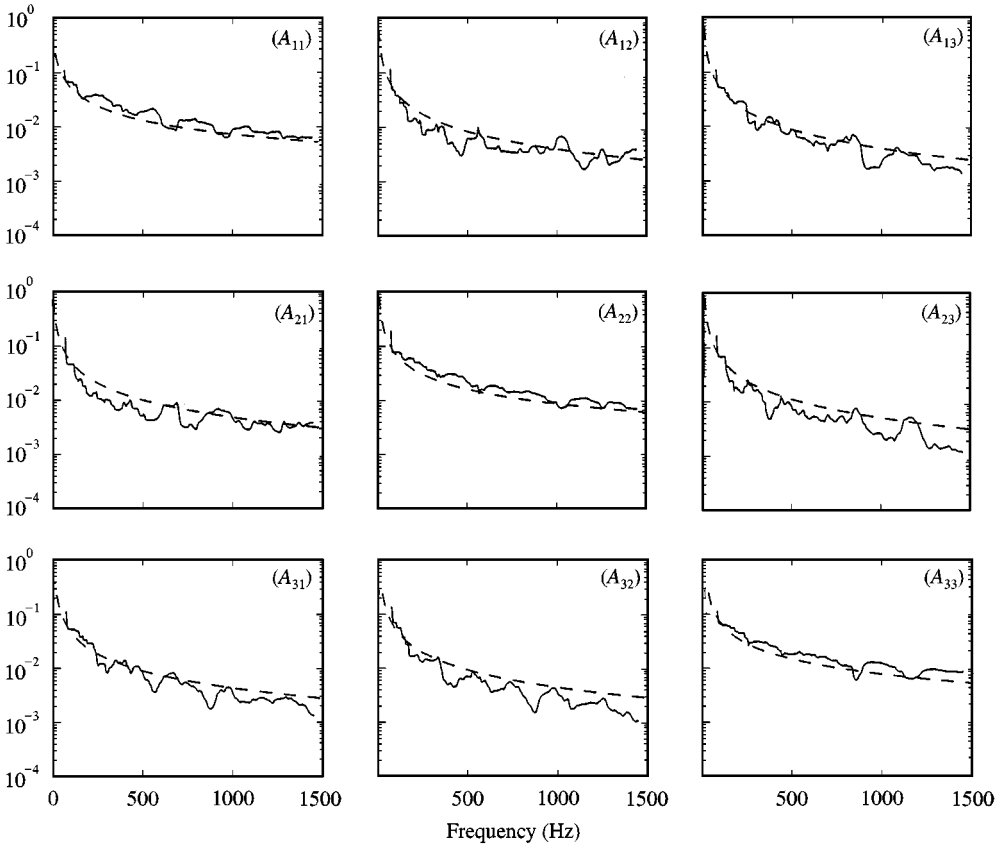

Figure 8. Frequency-averaged energy influence coefficients A_{ij} for the three-plate system, discrete frequency excitation (i, j indicated in upper right-hand corners of figures): —— 100 Hz frequency averages; – – – SEA predictions.

can be factored out and the frequency averaging performed independently; thirdly, because in many situations this frequency averaging can be performed analytically (and, in many cases, the light damping, broadband approximations of equations (24) and (25) give sufficient accuracy); and fourthly, because the component-mode approach *per se* substantially reduces the order of the model required to accurately perform the global modal analysis.

A numerical example of a system comprising three, edge-coupled, rectangular plates was then considered. Finite element/energy flow results were compared with traditional SEA predictions. Even when frequency-averaged (e.g., Figures 8 and 9), this example indicates potential applications of the method in two regards. First, there is a clear, non-smooth frequency dependence—this arises because the response is given in terms of mode-pair interactions, and in different frequency bands different numbers of modes interact and the strength by which they are coupled is also frequency-dependent: hence "exact", numerical results differ from the asymptotic averages of SEA. Secondly, "strong coupling" effects are evident, in that traditional SEA predictions themselves are inaccurate in this example—they underpredict the broadband response of the driven subsystem and overpredict the responses of the undriven ones: the asymptotic averages of SEA are themselves inaccurate.

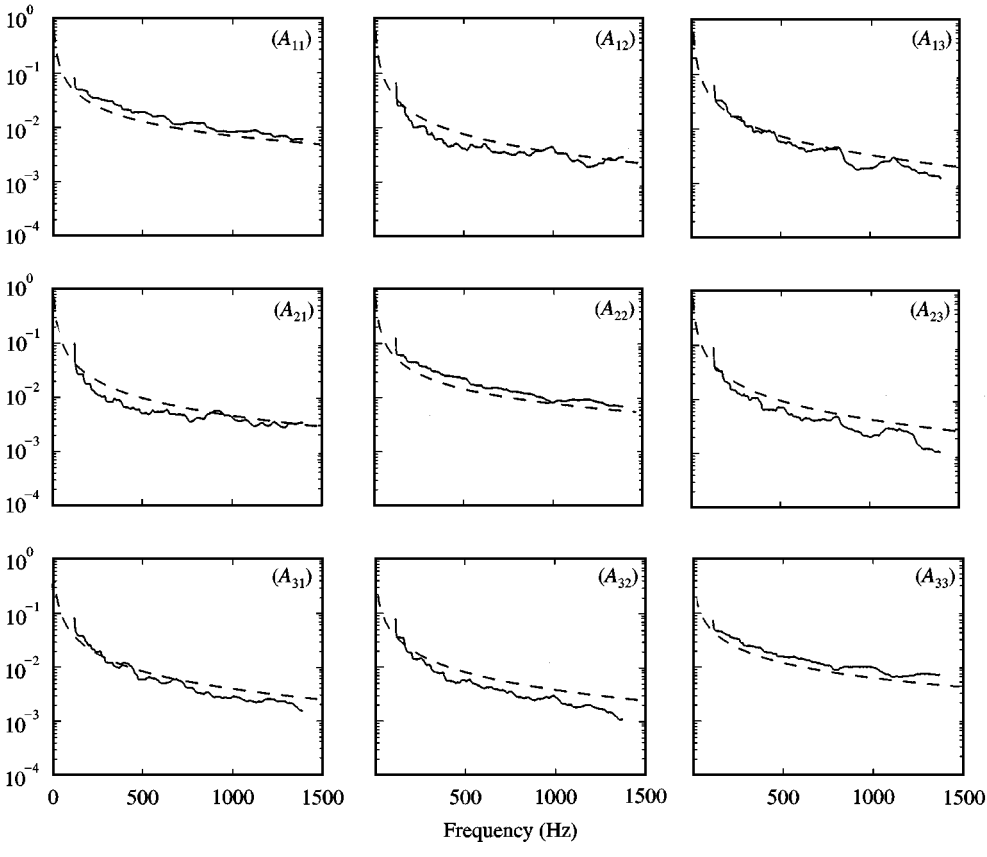

Figure 9. Frequency-averaged energy influence coefficients A_{ij} for the three-plate system, discrete frequency excitation (i, j indicated in upper right-hand corners of figures): —— 200 Hz frequency averages: – – – SEA predictions.

ACKNOWLEDGMENTS

The authors gratefully acknowledge the financial assistance provided by the New Zealand Foundation for Research, Science and Technology through Industrial Research Ltd. The research was undertaken while the second author held a University of Auckland Doctoral Scholarship.

REFERENCES

1. R. H. LYON 1975 *Statistical Energy Analysis of Vibrating Systems*. Cambridge, MA: MIT Press.
2. C. SIMMONS 1991 *Journal of Sound and Vibration* **144**, 215–227. Structure-borne sound transmission through plate junctions and estimates of SEA coupling loss factors using the FE method.
3. G. STIMPSON and N. LALOR 1992 *Internoise* **92**, 557–560. SEA extension of a F.E. model to predict total engine noise.
4. J. A. STEEL and R. J. M. CRAIK 1993 *Journal of Sound and Vibration* **178**, 553–561. Statistical energy analysis of structure-borne sound transmission by finite element methods.

5. K. SHANKAR and A. J. KEANE 1995 *Journal of Sound and Vibration* **181**, 801–838. A study of the vibrational energies of two coupled beams by finite element and green function (receptance) methods.
6. C. R. FREDÖ 1997 *Journal of Sound and Vibration* **199**, 645–666. SEA-like approach for the derivation of energy flow coefficients with a finite element model.
7. K. SHANKAR and A. J. KEANE 1995 *Journal of Sound and Vibration* **185**, 867–890. Energy flow predictions in a structure of rigidly joined beams using receptance theory.
8. K. SHANKAR and A. J. KEANE 1997 *Journal of Sound and Vibration* **201**, 491–513. Vibrational energy flow analysis using a substructure approach: the application of receptance theory to FEA and SEA.
9. E. H. DOWELL 1996 *Journal of Sound and Vibration* **194**, 445–447. Comment on energy flow predictions in a structure of rigidly joined beams using receptance theory.
10. S. A. HAMBRIC 1990 *Journal of Vibration and Acoustics* **112**, 542–549. Power flow and mechanical intensity calculations in structural finite element analysis.
11. L. GAVRIC and G. PAVIC 1993 *Journal of Sound and Vibration* **164**, 29–43. A finite element method for computation of structural intensity by the normal mode approach.
12. B. R. MACE 1994 *Journal of Sound and Vibration* **178**, 95–112. On the statistical energy analysis hypothesis of coupling power proportionality and some implications for its failure.
13. L. CREMER, M. HECKL and E. E. UNGAR 1988 *Structure-Borne Sound*. Berlin: Springer-Verlag, second edition.
14. R. R. CRAIG 1995 *Journal of Mechanical Design* **117B**, 207–213. Substructure methods in vibration.
15. R. R. CRAIG and M. C. BAMPTON 1968 *American Institute of Aeronautics and Astronautics Journal* **6**, 1313–1319. Coupling of substructures for dynamic analysis.
16. T. J. HUGHES and M. COHEN 1978 *Computers and Structures* **9**, 445–450. The heterosis finite element for plate bending.
17. B. R. MACE 1993 *Journal of Sound and Vibration* **166**, 429–461. The statistical energy analysis of two continuous one-dimensional subsystems.
18. E. C. N. WESTER and B. R. MACE 1996 *Journal of Sound and Vibration* **193**, 793–822. Statistical energy analysis of two edge-coupled rectangular plates: ensemble averages.

APPENDIX A: RAIN-ON-THE-ROOF EXCITATION

Consider an excitation $\mathbf{r}(x)$ that is delta-correlated in space. Since the excitation is delta correlated the total energy response can be calculated by calculating the response to excitation at a particular location x, and then integrating over all possible locations. Limiting attention to excitation within a particular element, the nodal forces that arise due to excitation at a point x_0 within the element are given by

$$\mathbf{F}^e = \int_v \mathbf{N}^{e\mathrm{T}}\mathbf{r}(x)\delta(x - x_0)\,\mathrm{d}v = \mathbf{N}^{e\mathrm{T}}\mathbf{r}(x_0), \tag{A.1}$$

where $\mathbf{N}^e$ is the matrix of element shape functions. From equation (17), the contribution to $\mathbf{A}$ is given by the following element matrix:

$$\mathbf{F}^{e*}\mathbf{F}^{e\mathrm{T}} = \mathbf{N}^{e\mathrm{T}}\mathbf{r}^*(x_0)\mathbf{r}^{\mathrm{T}}(x_0)\mathbf{N}^e. \tag{A.2}$$

Here it is assumed that the components of the point force are uncorrelated, with the magnitude in each direction being the same and given by $|\mathbf{r}(x_0)|$. Equation (A.2) then becomes

$$\mathbf{F}^{e*}\mathbf{F}^{e\mathrm{T}} = \mathbf{N}^{e\mathrm{T}}|\mathbf{r}(x_0)|^2. \tag{A.3}$$

Integrating over all possible excitation locations within the element gives

$$\mathbf{A}^e = \int_{x \in e} \mathbf{N}^{e\mathrm{T}} \mathbf{N}^e |\mathbf{r}(x)|^2 \, \mathrm{d}v. \tag{A.4}$$

Thus if $|\mathbf{r}(x)|^2 = R^2 \rho(x)$, where R^2 is a constant independent of space and $\rho(x)$ is the density, then the nodal forces are proportional to the consistent mass matrix for an element. By assembling the contributions from all other elements, it follows that the matrix $\mathbf{A} = R^2 \mathbf{M}_a$, where R^2 now gives the level of rain excitation in Newtons squared per unit volume. In this consistent formulation uncorrelated point forces give rise to coherent nodal forces. In practice, normally only small errors are introduced by assuming the nodal forces are uncorrelated and allocating nodal forces that are proportional to the mass lumped at each node.

APPENDIX B: FREQUENCY INTEGRALS IN CLOSED FORM

The integrals J_i over the frequency band Ω from ω_1 to ω_2, are given by

$$J_{1,m} = 2\mathrm{Re}\left\{ \frac{1}{(z_m - z_m^*)\sqrt{-z_m}} \arctan\left(\frac{B\sqrt{-z_m}}{\omega_1 \omega_2 - z_m} \right) \right\}, \tag{B.1}$$

$$J_{2,m} = 2\mathrm{e}\left\{ \frac{\sqrt{-z_m}}{(z_m - z_m^*)} \arctan\left(\frac{B\sqrt{-z_m}}{\omega_1 \omega_2 - z_m} \right) \right\}, \tag{B.2}$$

$$J_{3,n} = \frac{1}{2} \arctan\left(\frac{(\omega_2^2 - \omega_1^2)\eta\omega_m^2}{(\eta\omega_m^2)^2 + (\omega_2^2 - \omega_m^2)(\omega_1^2 - \omega_m^2)} \right), \tag{B.3}$$

$$J_{4,mp} = \frac{1}{(z_m - z_p)\sqrt{-z_m}} \arctan\left(\frac{B\sqrt{-z_m}}{\omega_1 \omega_2 - z_m} \right) + \frac{1}{(z_p - z_m)\sqrt{-z_p}} \arctan\left(\frac{B\sqrt{-z_p}}{\omega_1 \omega_2 - z_p} \right), \tag{B.4}$$

$$J_{5,mp} = \frac{\sqrt{-z_m}}{(z_p - z_m)} \arctan\left(\frac{B\sqrt{-z_m}}{\omega_1 \omega_2 - z_m} \right) + \frac{\sqrt{-z_p}}{(z_m - z_p)} \arctan\left(\frac{B\sqrt{-z_p}}{\omega_1 \omega_2 - z_p} \right), \tag{B.5}$$

where

$$z_m = \omega_m^2(1 - \mathrm{i}\eta); \qquad z_p = \omega_p^2(1 + \mathrm{i}\eta) \tag{B.6}$$

and the bandwidth $B = \omega_2 - \omega_1$. A two-quadrant arc-tangent function can be used to evaluate the integrals J_1, J_2, J_4 and J_5. When evaluating J_3 it is necessary to use a four-quadrant arc-tangent function. These integrals are only valid for non-zero natural frequencies, the contribution to the response from rigid-body modes is therefore neglected.

APPENDIX C: NOMENCLATURE

$\mathbf{A}$	nodal force matrix, $\mathbf{F}^{u*}\mathbf{F}^{u\mathrm{T}}$
B	bandwidth
$\mathbf{f}$	force vector
$\mathbf{F}$	force amplitude

$\mathbf{F}_{ab}$	coupling force
J_i	frequency integrals
$\mathbf{k}^u$	nodal stiffness matrix
$\mathbf{k}^q$	uncoupled component modal stiffness matrix
$\mathbf{k}^x$	coupled component modal stiffness matrix
$\mathbf{K}$	global stiffness matrix
$\mathbf{m}^u$	nodal mass matrix
$\mathbf{m}^q$	uncoupled component modal mass matrix
$\mathbf{m}^x$	coupled component modal mass matrix
$\mathbf{M}$	global mass matrix
$\mathbf{P}$	mode shape matrix
P_{ab}	coupling power between subsystems a and b
P_{diss}	dissipated power
P_{in}	input power
$\mathbf{q}$	uncoupled component modal degrees of freedom
R^2	constant, rain excitation level
$\mathbf{S}_b$	transformation matrix, equation (2)
S_{ff}	power spectral density
T	kinetic energy
$\mathbf{T}$	transformation matrix, equation (31)
$\mathbf{u}$	nodal degrees of freedom
$\mathbf{U}$	nodal amplitudes
V	potential energy
$\mathbf{x}$	coupled component modal degrees of freedom
$\mathbf{Y}$	global modal amplitudes
α	global modal receptance
$\boldsymbol{\beta}$	transformation matrix, equation (36)
Γ	mode pair receptance matrix, equation (20)
$\boldsymbol{\chi}$	constraint mode matrix
Ω	frequency band
$\boldsymbol{\phi}$	global mode shape
η	loss factor
$\boldsymbol{\kappa}_b$	stiffness distribution matrix associated with subsystem b
$\boldsymbol{\mu}_b$	mass distribution matrix associated with subsystem b
ω	excitation frequency
ω_0	centre frequency of frequency band
ω_1	lower frequency of frequency band
ω_2	upper frequency of frequency band
ω_j	jth natural frequency
$\boldsymbol{\psi}_a$	force distribution matrix associated with subsystem a

Subscripts

a, b, r	subsystem
i	interior degrees of freedom
c	coupling of degrees of freedom
∞	asymptotic, infinite value

Superscripts

u	nodal co-ordinates
q	uncoupled component modal co-ordinates
x	coupled component modal co-ordinates
Y	global modal co-ordinates.